Separation and Purification Technology 331 (2024) 125569

Contents lists available at ScienceDirect

Separation and Purification Technology

journal homepage: www.elsevier.com/locate/seppur

# Encrusting MOF nanoparticles onto nanofibers via spray-initiated synthesis to boost the filtration performances of nanofiber membranes

Ye Bian [a,1], Zhuolun Niu [b,1], Chencheng Zhang [a], Yue Pan [b], Yong Wang [a,*], Chun Chen [b,c,*]

[a] School of Energy and Environment, Southeast University, Nanjing 210096, China
[b] Department of Mechanical and Automation Engineering, The Chinese University of Hong Kong, Shatin, N.T. 999077, Hong Kong SAR, China
[c] Institute of Environment, Energy and Sustainability, The Chinese University of Hong Kong, Shatin, N.T. 999077, Hong Kong SAR, China

ARTICLE INFO

Editor: S. Yi

*Keywords:*
Spray-initiation
Metal-organic framework
Nanofiber filter
Submicron particles

ABSTRACT

Metal-organic frameworks (MOFs) are currently one of the most attractive porous materials. Integrating MOFs into an organic polymer matrix is considered a promising approach for controlling air pollutants. Especially, the nanoscale miniaturization of MOFs is promising to serve as membranes for efficient air quality control. Here, we proposed the use of spray-initiation as a facile and rapid methodology to assemble homogeneous growth of nanoMOFs on the electrospun fibers, yielding the composite fiber with diameters smaller than 300 nm. The developed ZIF-8-encrusted nanofiber membrane achieved superior filtration performance. Compared with the filter without MOF growth, the MOF-encrusted nanofiber filter achieved enhanced filtration efficiency and almost no change in pressure drop. For the most penetrating particles, the ZIF-8-encrusted nanofiber filter can even reach a 10% increment. This work shows that introducing the MOF nanoparticles onto the nanofibers with homogenous distribution can significantly improve the capacity of the filters in controlling submicron particles, and provide an important reference for the rational design of structures of composite materials.

## 1. Introduction

Metal-organic frameworks (MOFs), which are constructed by metal ions and organic linkers, have emerged as a class of porous organic-inorganic hybrid materials [1]. The structural features of MOFs endow them with adjustable pore size, high porosity, large surface area, and controllable functionalities, which are beneficial for the use in the control of air pollutants [2-5]. Although MOFs have attractive properties in air purification, most are obtained in powder form. The limitations of MOFs, such as poor processability and brittleness, also restrict the practical applications [6]. Embedding MOF powders into the flexible polymeric matrix to shape the MOF-polymer composites is appealing with great processability, chemical properties, and mechanical stabilities. More importantly, shaping MOFs as nanofiber structures with high surface-to-volume ratios enlarges the effective surface area in contact with the surrounding environment, which can increase the opportunity for air pollutants to be captured by the surface. Therefore, exploring MOF-functionalized membranes with enhanced separation performance is of great significance.

Among the polymeric fiber fabrication techniques, electrospinning is regarded as a versatile approach for the generation of nanofibers [7-9]. During the electrospinning process, the precursor electrospun solution is driven to the micro-needle, where a high voltage is applied to stretch the ejected jet into fine fibers. Electrospinning has been used to develop nanofibers from various organic polymers such as polyvinyl alcohol (PVA), polyvinyl pyrrolidone (PVP), polyacrylonitrile (PAN), nylon, polybenzimidazole (PBI), chitosan, poly(lactic acid) (PLA), polyurethane (PU) [10-18]. The diameters of nanofibers are comparable to the mean free path of air molecules. Therefore, the drag force can be significantly reduced due to the slip effect, which leads to the reduction of air resistance for nanofiber filters [19-21]. Recently, composite electrospun nanofibers, which are polymer matrix carrying dispersed organic or inorganic nanoparticles, have attracted great attention in air pollution control. Due to the good fiber-forming property, difficulty in hydrolysis, oxidation resistance, chemical stability, and good mechanical strength, PAN is favored in the selection as the substrate material. Also, the porous membrane structure and small diameter of PAN fiber can be easily controlled by tuning the electrospun parameters, which

* Corresponding authors at: School of Energy and Environment, Southeast University, Nanjing 210096, China(Y. Wang); Department of Mechanical and Automation Engineering, The Chinese University of Hong Kong, Shatin, N.T. 999077, Hong Kong SAR, China(C. Chen).
*E-mail addresses:* yongwang@seu.edu.cn (Y. Wang), chunchen@mae.cuhk.edu.hk (C. Chen).
[1] These authors contributed equally to this work.

https://doi.org/10.1016/j.seppur.2023.125569
Received 18 September 2023; Received in revised form 15 October 2023; Accepted 30 October 2023
Available online 31 October 2023

would be beneficial to achieving relatively high air permeability. Several functional materials can be incorporated into polymer nanofibers including nanostructured carbon-based materials, metal oxide nanoparticles, inorganic nanoparticles, MOFs, etc [22-26]. The integration of the above nanomaterials into nanofibers through the electrospinning process not only forms flexible membranes, but also achieves the superiority of both polymer matrix and introduced nanoparticles. Therefore, electrospinning is expected to shape MOF powders into flexible composite membranes with improved structural properties.

Generally, the development of MOF-incorporated electrospun nanofiber membrane can be divided into two main strategies, that is, direct electrospinning of MOF particles with polymer solutions [27-30], *in situ* growth of MOF particles on the developed electrospun fibers [31-34]. Direct electrospinning of MOF particles with polymer solutions is the most explored way to fabricate MOF-incorporated nanofibers, which applies to a wide range of MOFs. However, the diameters of the as-spun composite fibers are relatively large, which limits the airflow permeability. To overcome this challenge, the incorporation of metal-ion seeds into electrospun fibers to allow the *in situ* growth of MOF crystals can achieve low pressure drop. Nevertheless, same as the previous strategy, multistep and time-consuming fabrication processes hamper large-scale production. *In situ* growth of MOF particles during the electrospinning process is promising for achieving rapid growth of MOF nanoparticles into the fibers. However, a portion of MOF particles is buried inside the electrospun fiber, which is unable to participate in the control of air pollutants, therefore sacrificing the value of the whole MOF-incorporated nanofiber system. Consequently, there is still a great demand for developing efficient, rapid, and affordable strategies to fabricate MOF-incorporated nanofiber membranes with superior filtration performances.

In this work, we presented a rapid and facile spray-initiated strategy for preparing ZIF-8-encrusted nanofiber filters for effective fine particle control. The MOF nanoparticles can be uniformly encrusted onto metal-ion-doped electrospun fibers by spraying solutions of organic linkers. To confirm the benefit of the integrated ZIF-8 nanoparticles, the submicron particle filtration performance of electrospun fibers with and without encrusted MOFs was validated in detail. Moreover, the durability of the ZIF-8-encrusted nanofiber membranes for the filtration of fine particles during a month cycle was demonstrated. This spray-initiated synthesis strategy is expected to apply to prepare nanofiber membranes encrusted with different types of MOFs targeted for various applications.

## 2. Experimental section

### 2.1. Materials

Polyacrylonitrile (PAN, MW = 150,000 g $mol^{-1}$) was supplied by Sigma-Aldrich, USA. *N, N*-dimethylformamide (DMF, GC. 99.8%) was purchased from RCI Labscan, Thailand. 2-methylimidazole (2-MI, AR. 98%) and Zinc acetate dihydrate ($Zn(CH_3COO)_2{\cdot}2H_2O$, AR. 99%) were obtained from Aladdin Reagent, China.

### 2.2. Precursor electrospun fiber fabrication

First, the 6 wt% PAN solution (PAN/DMF) was prepared and magnetically stirred for 4 hr to form a homogenous solution. Next, Zn $(CH_3COO)_2{\cdot}2H_2O$ was dissolved into the prepared PAN solution and the mixed solution was stirred magnetically for one hr. The mass ratio between PAN and $Zn(CH_3COO)_2{\cdot}2H_2O$ was 2:1. The $Zn(CH_3COO)_2$ fiber was prepared using an electrospinning machine. The above-prepared precursor solution was driven by a syringe pump with a steady flow rate of 1 mL/h. A positive voltage of 10 kV was applied to the spinning needle. The developed fibers were collected using a grounded drum collector. The distance between the spinning needle and the collector was 20 cm.

### 2.3. ZIF-8-encrusted nanofiber membrane fabrication

First, 1% (w/v) 2-MI in ethanol solution was prepared. Next, the solution was transferred into a sprayer. Then, the organic linker solution was sprayed on the as-spun $Zn(CH_3COO)_2$/PAN membrane. ZIF-8 nanoparticles were formed after spraying the MI solution. After drying for 10 min, ethanol was used to wash the membrane to remove unreacted 2-MI.

### 2.4. Filtration performance test

The test particles were generated from a dust generator (RBG1000), namely Arizona test dust, which was mainly composed of silicon dioxide, aluminium oxide, iron trioxide, etc. In the filtration test, the airflow was set as 0.3 m/s and the actual filtration area of the filter was 36 $cm^2$. Two particle counters (TSI, 9306) with six testing channels, such as 0.3–0.4 μm, 0.4–0.5 μm, 0.5–0.7 μm, 0.7–1 μm, 1–2.5 μm, and >2.5 μm, were used to determine the filtration efficiency, which can be calculated using the following equation:

$$E = \frac{(C_1 - C_2)}{C_1} \quad (1)$$

where $C_1$ (#/L) and $C_2$ (#/L) are the particle number concentrations in the upstream and downstream direction of the filter, respectively. A manometer (TPI 621) with a resolution of 0.001 inches. of water was utilized to determine the pressure drop. The long-term test lasted for a month and simulated the application of the developed filters to be used within a practical living environment.

### 2.5. Characterization

The developed fibers were imaged by scanning electron microscopy (SEM, JEOL 7800F) and transmission electron microscopy (TEM, Tecnai F20). X-ray diffraction (XRD, SmartLab, Cu Kα1 radiation, $\lambda = 0.154$ nm, 40 kV, 30 mA) was conducted to determine the crystalline structure. The surface chemical species was studied by X-ray photoelectron spectroscopy (XPS, Escalab 250Xi). Brunauer-Emmet-Teller (BET) surface areas of the sample were measured by an $N_2$ adsorption and desorption test (ASAP 2460, Micromeritics).

## 3. Result and discussion

### 3.1. Spray-initiated synthesis of ZIF-8-encrusted nanofibers

This work proposed an easy and rapid spray-initiated synthesis strategy for the development of MOF-encrusted nanofiber membranes. To fully understand this methodology, we studied the formation of ZIF-8 nanoparticles on the electrospun fibers. As exhibited in Fig. 1, Zn $(CH_3COO)_2$/PAN nanofiber membrane was fabricated via the electrospinning technique first, which served as the MOF precursor membrane. Afterward, a sprayer containing 2-MI solution provided a steady feed rate to break the organic linker solution into small droplets, which subsequently contacted with $Zn(CH_3COO)_2$/PAN nanofiber membrane to realize the *in situ* growth of ZIF-8 on the surface of electrospun nanofiber. Differently, the growth of MOFs on the nanofiber in this study would happen at the air–solid interface. During the spray-initiated process, the evaporating droplet of organic linker shrank, contributing to increasing concentration at the fiber surface, until the critical organic linker concentration to react with $Zn^{2+}$ for the formation of ZIF-8 was reached. Next, the ZIF-8 began crystallizing at the air–solid interface. Upon droplet drying, more ZIF-8 nanoparticles were accumulated on the electrospun fiber surface accordingly. Consequently, the development of MOF-encrusted nanofiber membranes can be achieved within a short period, which is superior to the conventional time-consuming fabrication process. Therefore, the overall experimental procedure for

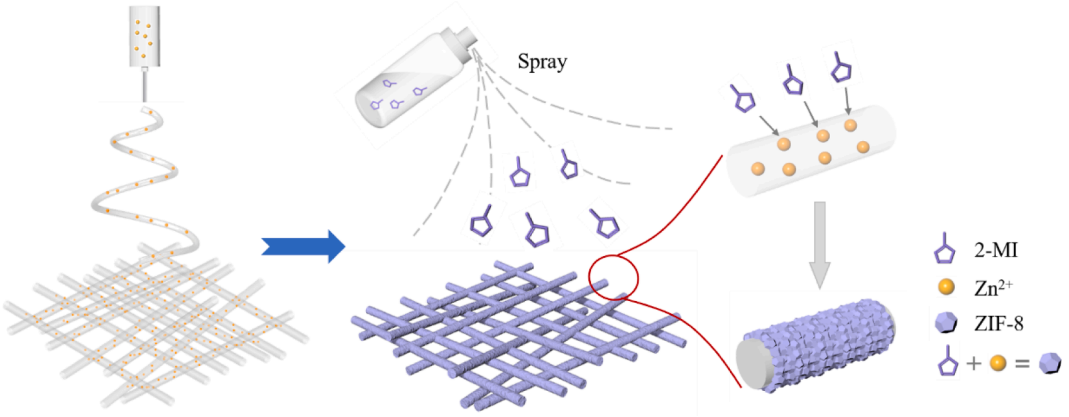


**Fig. 1.** Schematic showing of the development process for ZIF-8/PAN nanofiber membranes.

fabricating ZIF-8/PAN nanofiber is easy-operated at room temperature. Although the spray-initiated synthesis strategy achieved several superiorities for the development of MOF-encrusted nanofibers, the type of MOFs applicable for this strategy may be limited as it is performed with a mild synthesis process at room temperature. Therefore, those MOFs requiring elevated temperature for synthesis may not be suitable for this spray-initiated synthesis strategy.

### 3.2. Characterization of ZIF-8-encrusted nanofibers

The XRD patterns of ZIF-8 particles, PAN nanofiber membrane, and ZIF-8/PAN nanofiber filters can be observed in Fig. 2**a**. The XRD pattern of the as-spun ZIF-8/PAN membrane showed six peaks at 2θ range of 5 and 20°, which can be indexed to (011), (002), (112), (022), (013), and (222) diffractions [35,36]. Meanwhile, the surface chemical bonding states of PAN and ZIF-8/PAN were investigated by XPS. The spectra demonstrated that PAN and ZIF-8/PAN membranes both achieved the elements of O, N, and C. Differently, Zn only emerged in the ZIF-8/PAN membrane (Fig. 2**b**). A high-resolution Zn 2p orbit spectrum in Fig. 2**c** further depicted the peaks at 1044 and 1021 eV were attributed to Zn $2p_{1/2}$ and Zn $2p_{3/2}$, respectively. Both the XRD and XPS results indicated that the ZIF-8 particles were embedded on the composite membrane. Moreover, the BET surface area of the developed membranes was examined. The BET surface area of PAN nanofiber membrane and ZIF-8 was 10.6 $m^2/g$ (Fig. 2**d**) and 1760.5 $m^2/g$ (**Fig. S1**), respectively. With the integration of ZIF-8 on the nanofiber membrane, the BET surface area of ZIF-8/PAN came to 162.7 $m^2/g$. Although the BET surface area of ZIF-8/PAN was smaller than that of ZIF-8, there was an

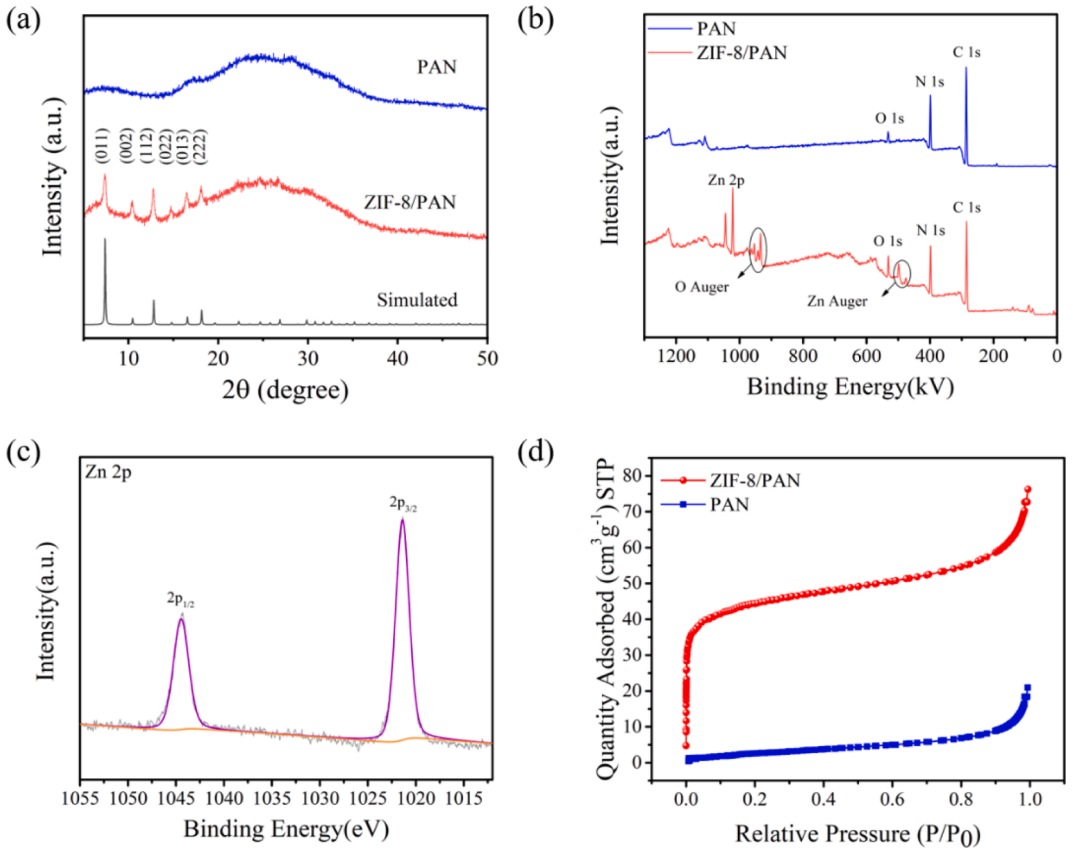


**Fig. 2.** (a) XRD spectra of pure PAN nanofiber, ZIF-8/PAN nanofiber, and simulated ZIF-8; (b) XPS survey spectra of ZIF-8/PAN nanofiber and PAN nanofiber; (c) high-resolution XPS spectrum of Zn 2p; (d) $N_2$ adsorption-desorption isotherms of ZIF-8/PAN nanofiber and PAN nanofiber.

interesting improvement compared to pure PAN nanofibers.

SEM was used to study the morphology of the as-developed electrospun nanofiber membranes. As shown in Fig. 3**a-b**, the morphology of pure PAN nanofiber was relatively smooth and the mean diameter was 297 nm (Fig. 3**c**). After the spray-initiated process, the ZIF-8 nanoparticles were generated and the synthesized ZIF-8/PAN nanofibers still achieved great uniformity and continuity (Fig. 3**d**). In Fig. 3**e**, the magnified SEM images exhibited that ZIF-8 nanoparticles were homogenously encrusted on the nanofibers. Moreover, the average diameter of the ZIF-8/PAN nanofibers (~294 nm) was comparable with that of PAN nanofibers (Fig. 3**f**). In addition, TEM images further depicted the growth of ZIF-8 nanoparticles on the electrospun nanofibers. As exhibited in Fig. 4**a-b,** uniform protrusions were distributed on the nanofibers after the incorporation of ZIF-8 nanoparticles. More importantly, ZIF-8 nanoparticles were observed to be anchored in the electrospun fiber, which indicates the tight interaction between MOFs and nanofibers. The thickness of MOF layers around the nanofibers was around 40 nm and could be tuned by controlling the concentration of metal ions inside the fiber. In addition, the linear scan profile as well as elemental mapping (Fig. 4**c-d**) demonstrated the homogeneous presence of Zn elements appeared in the electrospun nanofibers, which further confirmed the uniform distribution of ZIF-8 nanoparticles. Therefore, all the above structural and morphological characterizations confirmed that the developed spray-initiated method can successfully generate ZIF-8 nanoparticles on the electrospun nanofibers.

### 3.3. *Particle filtration performance of the ZIF-8-encrusted nanofiber filter*

The filtration performance of as-spun nanofiber filters was evaluated in a filtration testbed (**Fig. S2**). As can be seen in Fig. 5**a** and **Fig. S3**, the proposed ZIF-8/PAN nanofiber can capture the generated particles effectively. In Fig. 5**a**, the green square indicated the capture of large particles by the nanofiber network structure while the red circle showed the adhesion of tiny particles onto the ZIF-8/PAN nanofiber. To further demonstrate the PM collection ability of the developed nanofiber filter, the test particles were classified by aerodynamic diameter and defined as $PM_{0.3-0.4}$, $PM_{0.4-0.5}$, $PM_{0.5-0.7}$, $PM_{0.7-1}$, $PM_{1-2.5}$, and $PM_{>2.5}$, respectively.

To evaluate the advantage of ZIF-8 growth on the electrospun fiber via the spray-initiated synthesis method, the PAN nanofiber filter was selected for comparison. As shown in Fig. 5**b**, pure PAN and ZIF-8/PAN nanofiber filters achieved a common trend of filtration performance for particle capture. The filtration efficiency reached the lowest for particles with the smallest size and elevated with the increase of particle size. However, compared to PAN nanofibers, the ZIF-8/PAN nanofiber filter showed enhanced filtration efficiency for particles with almost all size ranges. Especially, the filtration efficiency improved more significantly for particle size below 0.5 μm. With the integration of ZIF-8 on the electrospun fibers, the composed nanofiber filter reached an enhancement of around 10% filtration efficiency, from 66% to 76.3% for $PM_{0.3-0.4}$. For particles with a diameter of 0.4–0.5 μm, the filtration efficiency achieved 83.9% and 77.1% for ZIF-8/PAN#1 and PAN#1, respectively. When the diameter of the particles was larger than 1 μm, the PM capture ability for filters with and without MOF growth was similar. The difference in filtration efficiency for various particle sizes can be explained as follows. First, the electrostatic interaction provided by ZIF-8 could play a key role in enhancing the capture of submicron particles [1,8,27,37-41]. According to Coulomb's law, the positive surface charges of ZIF-8 can increase the charge of fiber, which therefore enhances electrostatic force. Consequently, the enhanced electrostatic force can facilitate the adhesion of the tiny particles onto the surface of the hybrid fibers. Also, the homogeneous growth of ZIF-8 nanoparticles on the electrospun fiber would enhance the surface roughness, which could also benefit to capture of tiny particles [33,34]. For the control of large particles, the nanofiber network structure would be the dominant factor. Additionally, the pressure drop is also a significant factor in evaluating the filtration performance. Compared to a pure PAN nanofiber filter (118 Pa), the pressure drop of the filter after the integration of ZIF-8 slightly increased to 121 Pa, at a steady airflow velocity of 0.3 m/s. The comparable pressure drop can be attributed to the negligible increase in fiber diameter after the growth of ZIF-8 on PAN nanofiber, which was essential to affect the slip effect of the airstream around the fiber [21]. The quality factor (QF) could be quantified to the overall filtration performance for the filters, which was determined based on

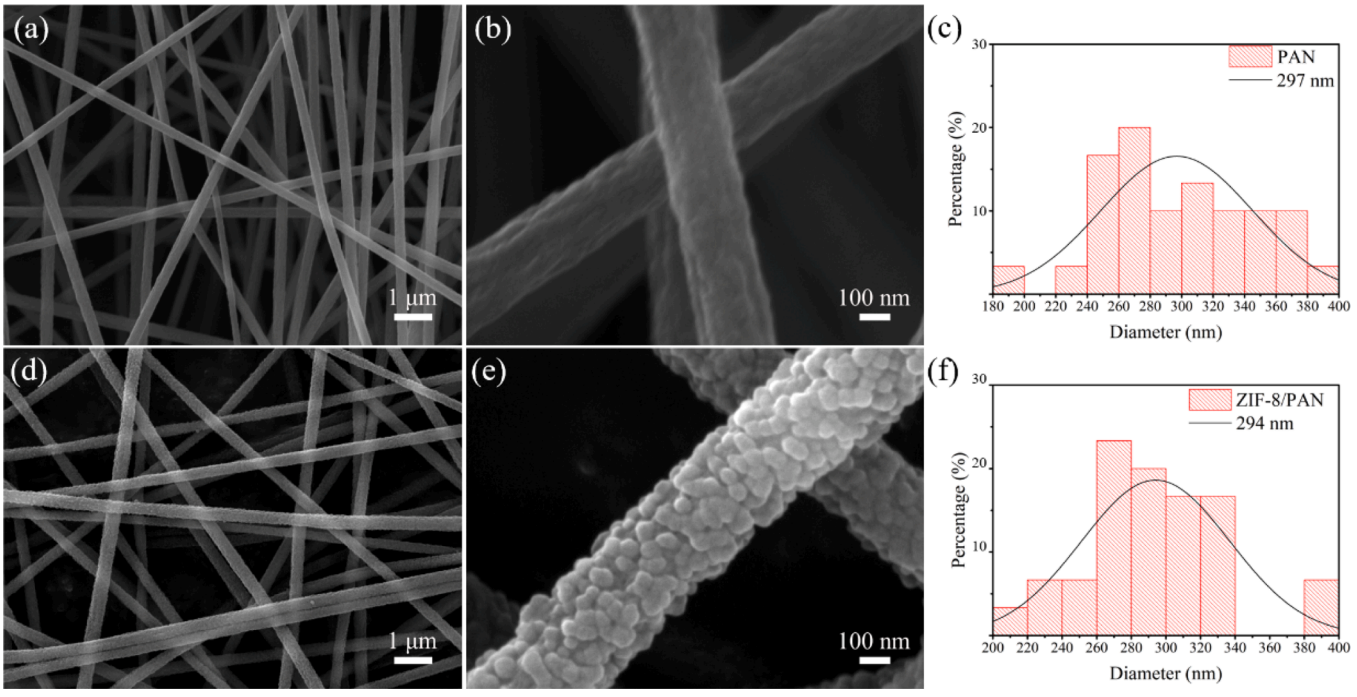


**Fig. 3.** (a-b) Microscopic images and (c) fiber diameter of the developed pure PAN nanofibers; (d-e) microscopic images and (f) fiber diameter of the developed ZIF-8/PAN nanofibers.

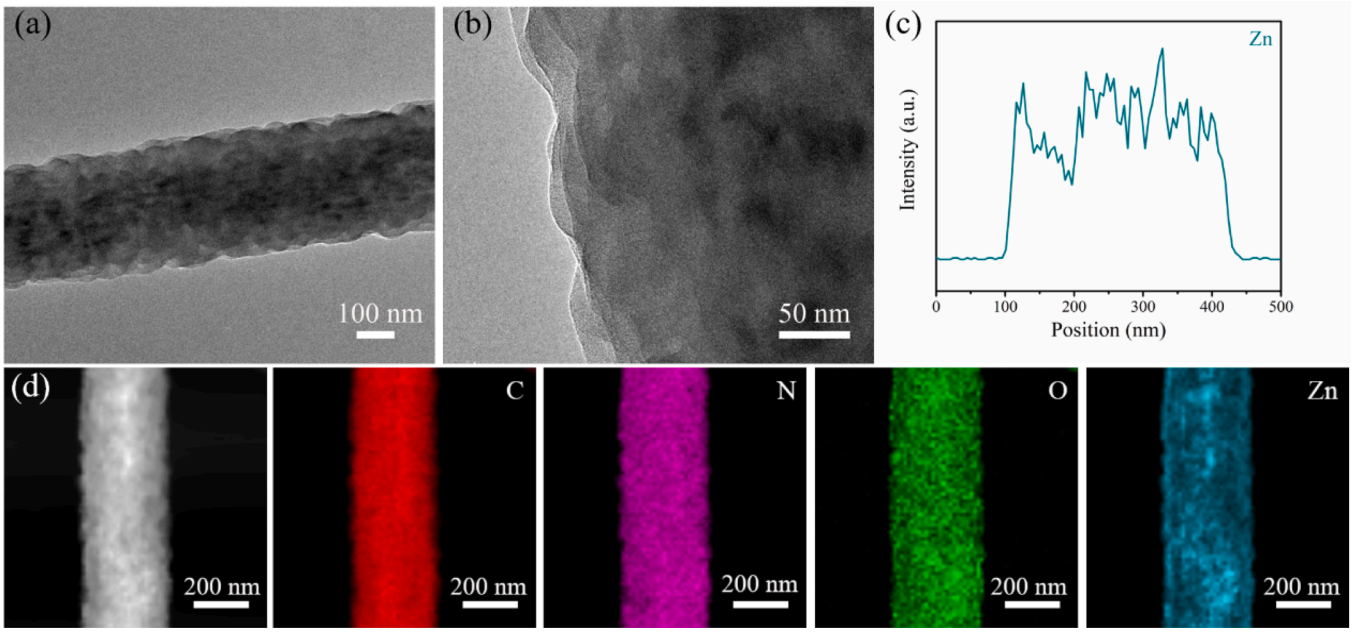


**Fig. 4.** (a-b) TEM images of ZIF-8/PAN membrane; (c) linear scan profile of ZIF-8/PAN nanofiber; (d) EDS elemental mapping of ZIF-8/PAN nanofiber.

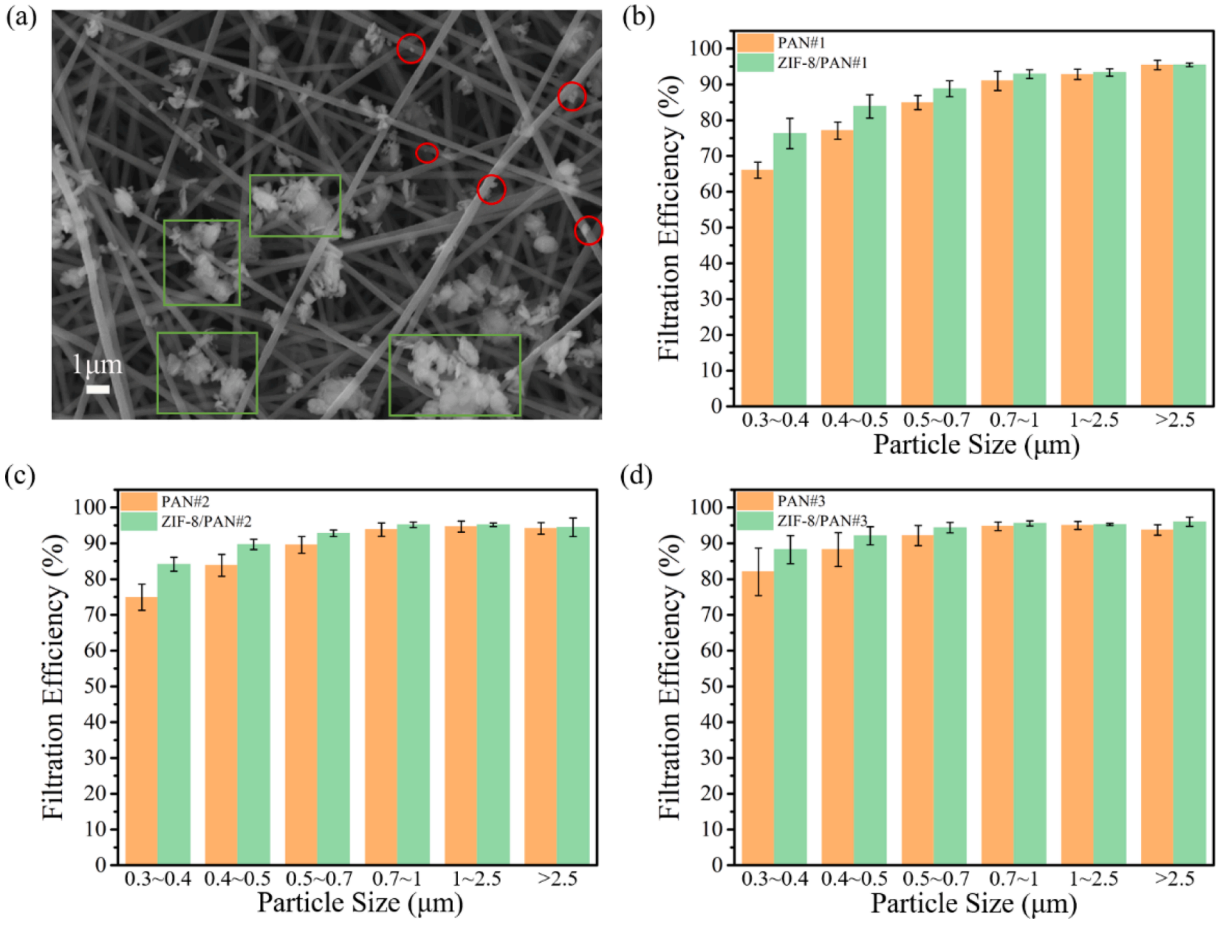


**Fig. 5.** (a) SEM image of the ZIF-8/PAN nanofiber membrane after filtration; subrange particle filtration efficiency for (b) PAN#1 and ZIF-8/PAN#1; (c) PAN#2 and ZIF-8/PAN#2; and (d) PAN#3 and ZIF-8/PAN#3.

both pressure drop and PM removal efficiency. Generally, the QF can be calculated using the following equation:

$$QF = \frac{-\ln(1 - E)}{\Delta P} \quad (2)$$

where E is the PM removal efficiency, and ΔP (Pa) is the pressure drop, respectively. The quality factor of the pure PAN#1 is 0.0092 while the ZIF-8/PAN#1 is 0.0119. The improvement of the quality factor value indicates the enhancement of the filtration performance by ZIF-8 modified membrane. To further demonstrate the superiority of the developed ZIF-8-encrusted filter in this work, a comparison of the air resistance coefficients between our work and the state-of-the-art MOF-based nanofiber filters was conducted. As shown in **Fig. S4**, with high filtration efficiency for submicron particles, the air resistance coefficient of our work is relatively lower than those of previous research.

In addition, the filtration performance of the as-spun filters with different thicknesses was evaluated, which can be seen in Fig. 5**b-d**. In this study, the membrane thickness was controlled by the regulation of electrospinning time. Both PAN and ZIF-8/PAN nanofiber filters achieved enhanced PM capture performance. However, the increased trend of filtration efficiency varied differently for particles with various size ranges. The filtration efficiency can achieve more enhancement for particles with smaller sizes. For example, ZIF-8/PAN#3 reached an enhancement of 12% for $PM_{0.3-0.4}$. For particles with aerodynamic diameters larger than 2.5 μm, the increased filtration efficiency was only around 0.5%, which can be explained by the classical filtration mechanisms. Inertial impaction and direct interception are the predominant mechanisms in capturing particles with large sizes [42]. Inertial impact refers to the inability of particles to adjust their trajectory and travel along their original path to hit the fiber. Generally, Stokes number (Stk) affects the single-fiber efficiency for inertial impaction, which can be defined as:

$$\mathrm{Stk} = \frac{C_c \rho_p d_p^2 U}{18 \mu d_f} \quad (3)$$

where $C_c$ (unitless) is the Cunningham coefficient, $\rho_p$ (kg/m$^3$) is the particle density, $d_p$ (m) is the diameter of the particle, μ (kg/ms) is the air dynamic viscosity, U (m/s) is the face velocity, and $d_f$ (m) is the diameter of the fiber. Direct interception occurs when the distance between the fiber surface and the particle is less than the particle radius. The interception performance of a single fiber can be determined by the ratio of particle diameter to fiber diameter (R, unitless), which can be expressed as follows:

$$R = \frac{d_p}{d_f} \quad (4)$$

where $d_p$ (m) and $d_f$ (m) are the particle diameter and the fiber diameter, respectively. According to Eqs. (3) and (4), larger particle diameter and smaller fiber diameter can result in higher Stk and R, which can contribute to strong effects of inertial impaction and direct interception. Therefore, the proposed nanofiber filter with small fiber diameters can still capture large particles effectively even if the membrane thickness is small.

When evaluating the applicability of a filter in practical applications, durability would be an essential parameter to be considered. The durability test was studied in a real application scenario under mild wind for a month. The schematical showing of the durable filtration process is depicted in Fig. 6**a**. Clean air can be achieved accordingly with the use of the developed filter. The filtration results of the ZIF-8/PAN nanofiber filter were given in Fig. 6**b**, showing that the filtration performance for particles with a diameter above 0.7 μm was stable during the whole long-term test. The steady capture ability can be attributed to both inertial impaction and interception mechanisms. However, the capture efficiency of particles with a diameter smaller than 0.7 μm underwent an elevation in the first ten days and then became stable in the following filtration process. For tiny particles, especially the most penetration particles, the predominant mechanism was the electrostatic interaction of ZIF-8 on the composed fibers. Also, the filtration ability was supposed to decline since the electrostatic interaction became weaker with the prolonging of the filtration duration. However, the captured dust attached continuously to the fiber surface during the long-term test, which served as another filtration media for PM capture, resulting in increased filtration efficiency.

## 4. Conclusions

In summary, we proposed a spray-initiated synthesis strategy for the development of a ZIF-8-encrusted nanofiber membrane. This approach is facile and rapid, and drastically reduces production times and costs. Given the synthetic conditions offered by spray-initiated, nanoMOFs can be synthesized and homogenously embedded into the electrospun fiber. Especially, the generation of ZIF-8 nanoparticles on the fiber resulted in a negligible impact on the increase of fiber diameter. The filtration results confirmed that the developed ZIF-8-encrusted nanofiber filter can capture submicron particles effectively. After generating ZIF-8 nanoparticles on the electrospun fibers, the filtration efficiency increased by 10% for the most penetrating particles. Meanwhile, the pressure drop remained stable due to the almost unchanged fiber diameter after MOF growth. In addition, the developed ZIF-8-encrusted nanofiber filter

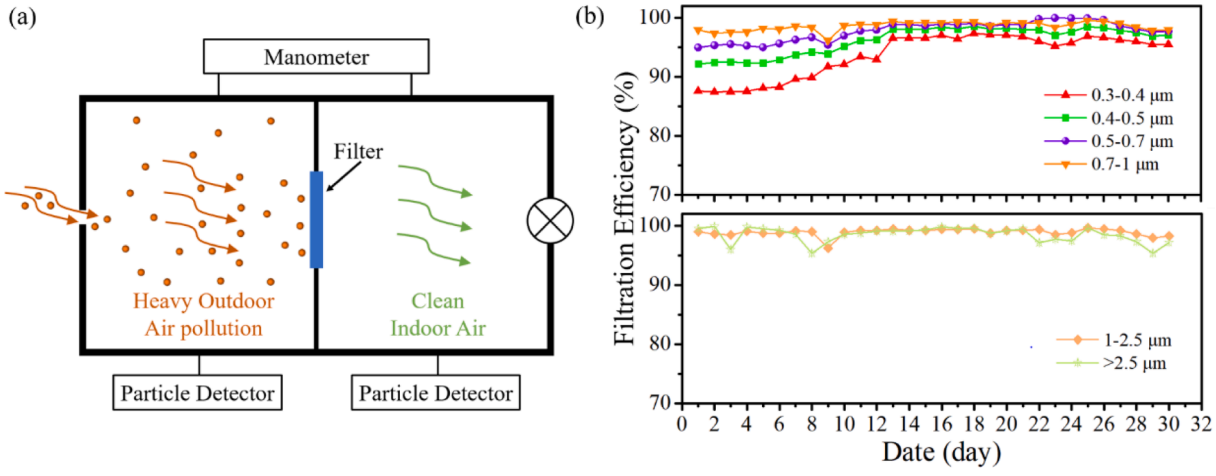


**Fig. 6.** (a) Schematic representation for the test of developed filters in a real application scenario; (b) long-term filtration results of the ZIF-8/PAN nanofiber.

exhibited durable service life in a real application scenario. Overall, this study provides a promising strategy for the development of ZIF-8-encrusted nanofiber membranes using a rapid and efficient process, which may shed light on the design of MOF-encrusted nanofibrous heterostructures.

## CRediT authorship contribution statement

**Ye Bian:** Investigation, Methodology, Writing – original draft. **Zhuolun Niu:** Methodology. **Chencheng Zhang:** Writing – review & editing. **Yue Pan:** Methodology. **Yong Wang:** Supervision, Writing – review & editing, Conceptualization. **Chun Chen:** Conceptualization, Funding acquisition, Writing – review & editing.

## Declaration of Competing Interest

The authors declare that they have no known competing financial interests or personal relationships that could have appeared to influence the work reported in this paper.

## Data availability

Data will be made available on request.

## Acknowledgements

This work was supported by the Natural Science Foundation of Jiangsu Province of China (BK20220863), the 2021 High-level Personnel Project Funding of Jiangsu Province JSSCBS20210053, the General Research Fund of Research Grants Council of Hong Kong SAR, China (Grant No. 14204520 and 14221122), and the InnoHK of the Government of Hong Kong via the Hong Kong Centre for Logistics Robotics, Hong Kong SAR, China.

## Appendix A. Supplementary data

Supplementary data to this article can be found online at https://doi.org/10.1016/j.seppur.2023.125569.

## References

[1] J. Mao, Y. Tang, Y. Wang, J. Huang, X. Dong, Z. Chen, Y. Lai, Particulate Matter Capturing via Naturally Dried ZIF-8/Graphene Aerogels under Harsh Conditions, IScience 16 (2019) 133–144.
[2] L. Xie, X. Liu, L. Xie, X. Liu, T. He, J. Li, Metal-Organic Frameworks for the Capture of Trace Aromatic Volatile Organic Compounds Metal-Organic Frameworks for the Capture of Trace Aromatic Volatile Organic Compounds, Chem 4 (2018) 1911–1927.
[3] P. Li, J. Li, X. Feng, J. Li, Y. Hao, J. Zhang, H. Wang, A. Yin, J. Zhou, X. Ma, B. Wang, Metal-organic frameworks with photocatalytic bactericidal activity for integrated air cleaning, Nat. Commun. 10 (2019) 2177.
[4] M. Lee, G.P. Ojha, H.J. Oh, T. Kim, H.Y. Kim, Copper//terbium dual metal organic frameworks incorporated side-by-side electrospun nanofibrous membrane: A novel tactics for an efficient adsorption of particulate matter and luminescence property, J. Colloid Interface Sci. 578 (2020) 155–163.
[5] H.C. Woo, D.K. Yoo, S.H. Jhung, Highly Improved Performance of Cotton Air Filters in Particulate Matter Removal by the Incorporation of Metal-Organic Frameworks with Functional Groups Capable of Large Charge Separation, ACS Appl. Mater. Interfaces 12 (2020) 28885–28893.
[6] F. Ahmadijokani, H. Molavi, A. Bahi, R. Fernández, P. Alaee, S. Wu, S. Wuttke, F. Ko, M. Arjmand, Metal-Organic Frameworks and Electrospinning: A Happy Marriage for Wastewater Treatment, Adv. Funct. Mater. 32 (2022) 2207723.
[7] J. Xiao, J. Liang, C. Zhang, Y. Tao, G. Ling, Q. Yang, Advanced Materials for Capturing Particulate Matter : Progress and Perspectives, Small Methods 2 (2018) 1800012.
[8] H. Liu, C. Cao, J. Huang, Z. Chen, G. Chen, Y. Lai, Progress on particulate matter filtration technology: Basic concepts, advanced materials, and performances, Nanoscale 12 (2020) 437–453.
[9] T. Lu, J. Cui, Q. Qu, Y. Wang, J. Zhang, R. Xiong, W. Ma, C. Huang, Multistructured Electrospun Nanofibers for Air Filtration: A Review, ACS Appl. Mater. Interfaces 13 (2021) 23293–23313.
[10] F. Zuo, S. Zhang, H. Liu, H. Fong, X. Yin, J. Yu, B. Ding, Free-Standing Polyurethane Nanofiber/Nets Air Filters for Effective PM Capture, Small 13 (2017) 1702139.
[11] D. Lv, M. Zhu, Z. Jiang, S. Jiang, Q. Zhang, R. Xiong, C. Huang, Green Electrospun Nanofibers and Their Application in Air Filtration, Macromol. Mater. Eng. 303 (2018) 1800336.
[12] Y. Bian, R. Wang, S.H. Ting, C. Chen, L. Zhang, Electrospun SF/PVA Nanofiber Filters for Highly Efficient PM2.5 Capture, IEEE Trans. Nanotechnol. 17 (2018) 934–939.
[13] S. Lee, A.R. Cho, D. Park, J.K. Kim, K.S. Han, I.J. Yoon, M.H. Lee, J. Nah, Reusable Polybenzimidazole Nanofiber Membrane Filter for Highly Breathable PM2.5 Dust Proof Mask, ACS Appl. Mater. Interfaces 11 (2019) 2750–2757.
[14] Z. Niu, Y. Bian, T. Xia, L. Zhang, C. Chen, An optimization approach for fabricating electrospun nanofiber air filters with minimized pressure drop for indoor PM2.5 control, Build. Environ. 188 (2021), 107449.
[15] L. Wang, Y. Bian, C.K. Lim, Z. Niu, P.K.H. Lee, C. Chen, L. Zhang, W.A. Daoud, Y. Zi, Tribo-charge enhanced hybrid air filter masks for efficient particulate matter capture with greatly extended service life, Nano Energy 85 (2021), 106015.
[16] L. Wang, Y. Gao, J. Xiong, W. Shao, C. Cui, N. Sun, Y. Zhang, S. Chang, P. Han, F. Liu, J. He, Biodegradable and high-performance multiscale structured nanofiber membrane as mask filter media via poly(lactic acid) electrospinning, J. Colloid Interface Sci. 606 (2022) 961–970.
[17] W. Han, D. Rao, H. Gao, X. Yang, H. Fan, C. Li, L. Dong, H. Meng, Green-solvent-processable biodegradable poly(lactic acid) nanofibrous membranes with bead-on-string structure for effective air filtration: "Kill two birds with one stone", Nano Energy 97 (2022), 107237.
[18] Y. Bian, C. Zhang, H. Wang, Q. Cao, Degradable nanofiber for eco-friendly air filtration : Progress and perspectives, Sep. Purif. Technol. 306 (2023), 122642.
[19] X. Zhao, S. Wang, X. Yin, J. Yu, B. Ding, Slip-Effect Functional Air Filter for Efficient Purification of PM 2.5, Sci. Rep. 6 (2016) 35472.
[20] T. Xia, Y. Bian, L. Zhang, C. Chen, Relationship between pressure drop and face velocity for electrospun nanofiber filters, Energy Build. 158 (2018) 987–999.
[21] Y. Bian, L. Zhang, C. Chen, Experimental and modeling study of pressure drop across electrospun nano fiber air filters, Build. Environ. 142 (2018) 244–251.
[22] Q. Zhu, X. Tang, S. Feng, Z. Zhong, J. Yao, Z. Yao, ZIF-8@SiO2 composite nanofiber membrane with bioinspired spider web-like structure for efficient air pollution control, J. Memb. Sci. 581 (2019) 252–261.
[23] F. Liu, M. Li, W. Shao, W. Yue, B. Hu, K. Weng, Y. Chen, X. Liao, J. He, Preparation of a polyurethane electret nanofiber membrane and its air-filtration performance, J. Colloid Interface Sci. 557 (2019) 318–327.
[24] D. Lv, R. Wang, G. Tang, Z. Mou, J. Lei, J. Han, S. De Smedt, R. Xiong, C. Huang, Ecofriendly Electrospun Membranes Loaded with Visible-Light-Responding Nanoparticles for Multifunctional Usages: Highly Efficient Air Filtration, Dye Scavenging, and Bactericidal Activity, ACS Appl. Mater. Interfaces 11 (2019) 12880–12889.
[25] M. Essalhi, M. Khayet, S. Tesfalidet, M. Alsultan, N. Tavajohi, Desalination by direct contact membrane distillation using mixed matrix electrospun nanofibrous membranes with carbon-based nanofillers: A strategic improvement, Chem. Eng. J. 426 (2021), 131316.
[26] Y. Gao, E. Tian, Y. Zhang, J. Mo, Utilizing electrostatic effect in fibrous filters for efficient airborne particles removal: Principles, fabrication, and material properties, Appl. Mater. Today 26 (2022), 101369.
[27] Y. Zhang, S. Yuan, X. Feng, H. Li, J. Zhou, B. Wang, Preparation of nanofibrous metal-organic framework filters for efficient air pollution control, J. Am. Chem. Soc. 138 (2016) 5785–5788.
[28] Z. Wang, Y. Zhang, X.Y.D. Ma, J. Ang, Z. Zeng, B.F. Ng, M.P. Wan, S.C. Wong, X. Lu, Polymer/MOF-derived multilayer fibrous membranes for moisture-wicking and efficient capturing both fine and ultrafine airborne particles, Sep. Purif. Technol. 235 (2020), 116183.
[29] M. Hu, L. Yin, N. Low, D. Ji, Y. Liu, J. Yao, Z. Zhong, W. Xing, Zeolitic-imidazolate-framework filled hierarchical porous nanofiber membrane for air cleaning, J. Memb. Sci. 594 (2020), 117467.
[30] Z. Hao, J. Wu, C. Wang, J. Liu, Electrospun Polyimide/Metal-Organic Framework Nanofibrous Membrane with Superior Thermal Stability for Efficient PM 2.5 Capture, ACS Appl. Mater. Interfaces 11 (2019) 11904–11909.
[31] Y. Bian, R. Wang, S. Wang, C. Yao, W. Ren, C. Chen, L. Zhang, Metal-organic framework-based nanofiber filters for effective indoor air quality control, J. Mater. Chem. A 6 (2018) 15807–15814.
[32] C. Wang, T. Zheng, R. Luo, C. Liu, M. Zhang, J. Li, X. Sun, J. Shen, W. Han, L. Wang, In Situ Growth of ZIF-8 on PAN Fibrous Filters for Highly Efficient U(VI) Removal, ACS Appl. Mater. Interfaces 10 (2018) 24164–24171.
[33] Y. Bian, C. Chen, R. Wang, S. Wang, Y. Pan, B. Zhao, C. Chen, L. Zhang, Effective removal of particles down to 15 nm using scalable metal-organic framework-based nanofiber filters, Appl. Mater. Today 20 (2020), 100653.
[34] Y. Bian, Z. Niu, S. Wang, Y. Pan, L. Zhang, C. Chen, Removal of Size-Dependent Submicron Particles Using Metal-Organic Framework-Based Nanofiber Air Filters, ACS Appl. Mater. Interfaces 14 (2022) 23570–23576.
[35] W. Morris, C.J. Stevens, R.E. Taylor, C. Dybowski, O.M. Yaghi, M.A. Garcia-Garibay, NMR and X-ray study revealing the rigidity of zeolitic imidazolate frameworks, J. Phys. Chem. C. 116 (2012) 13307–13312.
[36] Y. Wang, H. Song, C. Liu, Y. Zhang, Y. Kong, J. Tang, Y. Yang, C. Yu, Confined growth of ZIF-8 in dendritic mesoporous organosilica nanoparticles as bioregulators for enhanced mRNa delivery in vivo, Natl. Sci. Rev. 8 (2021) nwaa268.

[37] Y. Chen, S. Zhang, S. Cao, S. Li, F. Chen, S. Yuan, C. Xu, J. Zhou, X. Feng, X. Ma, B. Wang, Roll-to-Roll Production of Metal-Organic Framework Coatings for Particulate Matter Removal, Adv. Mater. 29 (2017) 1606221.
[38] X. Ma, Y. Chai, P. Li, B. Wang, Metal-Organic Framework Films and Their Potential Applications in Environmental Pollution Control, Acc. Chem. Res. 52 (2019) 1461–1470.
[39] H. Xiao, Z.X. Low, D.B. Gore, R. Kumar, M. Asadnia, Z. Zhong, Porous metal–organic framework-based filters: Synthesis methods and applications for environmental remediation, Chem. Eng. J. 430 (2022), 133160.
[40] Z. Wang, F. Yin, X.F. Zhang, T. Zheng, J. Yao, Delignified wood filter functionalized with metal-organic frameworks for high-efficiency air filtration, Sep. Purif. Technol. 293 (2022), 121095.
[41] C. Zhu, F. Yang, T. Xue, Q. Wali, W. Fan, T. Liu, Metal-organic framework decorated polyimide nanofiber aerogels for efficient high-temperature particulate matter removal, Sep. Purif. Technol. 300 (2022), 121881.
[42] Y. Bian, S. Wang, L. Zhang, C. Chen, Influence of fiber diameter, filter thickness, and packing density on PM2.5 removal efficiency of electrospun nanofiber air filters for indoor applications, Build. Environ. 170 (2020), 106628.